RESEARCH PAPER

Synthesis, and Morphological Characterization of TiO_2-Based Nano-Composite for Antimicrobial Applications

Muayad Raheem Hussein[1], Sabah Hasan Jumaah[2,*], Ali N. Majeed[3]

* *boshrags@yahoo.com*

[1] University of sumer, college of science, physics department, Thi-Qar, Iraq
[2] Mustansiriyah university, college of science, physics department, Baghdad, Iraq
[3] Scientific Research Commission, Baghdad, Iraq

Received: Augest 2025 **Revised: November 2025** **Accepted: December 2025**
DOI: 10.22068/ijmse.4261

Abstract: *In the current study, titanium dioxide (TiO_2) nanoparticles were synthesised and subsequently combined with chitosan (CS) and silver (Ag) to enhance their antimicrobial activity. The synthesised TiO_2, TiO_2-CS, and TiO_2-CS-Ag nanocomposites were characterised using various techniques to thoroughly assess their structural, morphological, and compositional properties. XRD analysis substantiated the phase transition from anatase to rutile upon incorporation of chitosan and silver, accompanied by a reduction in nanoparticle dimensions. FTIR spectra corroborated the presence of functional groups associated with chitosan and silver, while FESEM revealed morphological modifications, notably the emergence of polygonal nanostructures within the TiO_2-CS-Ag composite. The antibacterial efficacy of the synthesized nanocomposites was evaluated against Escherichia coli (E.coli) and Staphylococcus aureus (S.aureus). Although pure TiO_2 showed minimal antibacterial activity, the TiO_2-CS and TiO_2-CS-Ag composites exhibited substantial inhibition zones, with the TiO_2-CS-Ag composite showing the greatest efficacy, attributable to the synergistic interaction between chitosan and silver nanoparticles. BET analysis revealed that the augmented antimicrobial activity was associated with the increased surface area of the TiO_2-CS-Ag nanocomposite.*

Keywords: *TiO_2 nanocomposite, Chitosan, Silver nanoparticles, Antibacterial activity, Green synthesis, Morphological characterization.*

1. INTRODUCTION

Nanotechnology has enabled the development of advanced materials with superior physicochemical properties applicable across diverse biomedical and environmental fields. Among these innovative materials, titanium dioxide (TiO_2)-based nano-composites have emerged as a focal point of research due to their remarkable photocatalytic, antibacterial, and biocompatible attributes [1, 2]. TiO_2 nanoparticles have found extensive application in antimicrobial coatings, water purification processes, and biomedical devices, primarily owing to their capability to produce reactive oxygen species (ROS) upon light exposure, which effectively eradicates microbial pathogens [3, 4]. Nonetheless, unmodified TiO_2 nanoparticles are constrained by several limitations, including insufficient surface area, the recombination of electron-hole pairs, and restricted activity under visible light irradiation [5]. To address these limitations, composite formulations integrating biopolymers and metallic nanoparticles have been investigated to bolster antimicrobial effectiveness and stability [6].

Chitosan (CS), a naturally occurring biopolymer sourced from chitin, has been the subject of extensive scholarly investigation due to its biocompatibility, biodegradability, and inherent antimicrobial properties. The functionalization of chitosan with TiO_2 nanoparticles engenders synergistic antimicrobial effects by facilitating the disruption of bacterial cell membranes while augmenting ROS generation [7, 8]. Furthermore, silver (Ag) nanoparticles are recognised for their broad-spectrum antimicrobial activities, which are attributed to their ability to interact with bacterial cell walls, generate ROS, and interfere with cellular metabolic processes [9, 10]. The integration of Ag nanoparticles into TiO_2-CS nanocomposites is hypothesised to enhance antimicrobial efficacy and sustain bioactivity [11, 12].

Several studies have demonstrated that modification of TiO_2 with biopolymers and metallic nanoparticles not only enhances its surface characteristics but also facilitates the controlled release of antimicrobial agents while augmenting its biocidal efficacy against both Gram-positive and Gram-negative bacteria [13, 14]. In this regard, Hoang et al. fabricated polyvinyl alcohol (PVA)/CS/TiO_2@Ag nanofiber using the electrospinning technique in

[DOI: 10.22068/ijmse.4261]

order to examine its antibacterial activity against Escherichia coli (E.coli) and Staphylococcus aureus (S.aureus) bacteria. The results showed that the resultant nanofiber shows appropriate antibacterial activity against both bacteria [15]. In another study, a fish gelatin/CS/TiO_2-Ag composite showing high antibacterial activity was prepared. Because of its antibacterial activity, the composite was expected to be a suitable candidate for the food packaging industry [16].

Owing to the abovementioned properties, the current study endeavours to prepare TiO_2-CS and TiO_2-CS-Ag nanocomposites and characterize their morphology and structure by means of X-ray diffraction (XRD), Fourier-transform infrared spectroscopy (FTIR), field-emission scanning electron microscopy (FESEM), energy-dispersive X-ray spectroscopy (EDXS), Brunauer-Emmett-Teller (BET), and Barrett-Joyner-Halenda (BJH). Moreover, the antibacterial activity of the synthesised nanocomposites will be rigorously evaluated against E.coli and S.aureus bacteria to ascertain their antimicrobial efficacy.

2. EXPERIMENTAL PROCEDURES

2.1. Preparation of TiO_2 Nanoparticles

TiO_2 nanoparticles were synthesized utilizing the hydrothermal technique. Initially, a precursor solution was formulated by combining 5 mL of ethanol with 5 mL of acetic acid under magnetic agitation for 15 min. Subsequently, 5 mL of titanium tetraisopropoxide (TTIP) was added dropwise, followed by continuous stirring for an additional 15 min to facilitate the hydrolysis of the precursor. To initiate the hydrolysis reaction, 100 mL of deionised water was rapidly added, followed by 2 mL of concentrated nitric acid. The resultant solution was heated under reflux at 80°C for 1 hour, during which a colour transition from white to pale blue was observed.

For the hydrothermal treatment, the solution was transferred into a 100 mL stainless steel autoclave equipped with a Teflon liner to ensure chemical inertness. The autoclave was hermetically sealed and heated to 200°C for 10 hours to facilitate the formation of nanoparticles under meticulously controlled temperature and pressure conditions. Upon completion, the mixture was centrifuged at 10,000 rpm for 5 min to isolate the solid phase, which was then washed 3 times with ethanol. The resulting precipitate was dried at 60°C in an oven and subsequently ground into a fine powder for further characterization.

2.2. Preparation of TiO_2-CS Nanocomposite

A chitosan solution was formulated by solubilising 0.5 g of chitosan powder in 50 mL of deionised water, augmented with 0.5 mL of acetic acid, at 80°C for 30 min. In a separate procedure, 0.5 g of TiO_2 nanoparticles was uniformly dispersed in 50 mL of deionized water while being agitated for 30 min. Subsequently, the two resultant solutions were combined and heated at 70°C for 15 min to obtain a homogeneous mixture.

2.3. Preparation of TiO_2-CS-Ag Nanocomposite

In order to fabricate TiO_2-CS-Ag nanocomposite, in addition to the preparation of two solutions in section 2.2, a separate silver precursor solution was formulated by dissolving 0.1 g of silver nitrate in 10 mL of deionised water under continuous agitation at ambient temperature. The three resultant solutions were combined and heated at 70°C for 15 min to ensure a uniform mixture.

2.4. Implant Coating Procedure

Titanium skull mesh implants were coated using the dip-coating technique with a dip-coating device from Iranian Toos Nano. The implants were systematically immersed in the prepared TiO_2, TiO_2-CS, and TiO_2-CS-Ag solutions at a meticulously controlled immersion rate of 10 mm/min. Each cycle comprised a 10-second immersion followed by a 5-min drying interval, and this process was reiterated for a total of 50 cycles. After the coating procedure, the samples were dried in an oven at 120 °C for 24 hours to ensure complete adhesion of the coating layers.

3. RESULTS AND DISCUSSION

3.1. Characterization Analyses

Figure 1 demonstrates the XRD patterns of TiO_2, TiO_2-CS, and TiO_2-CS-Ag recorded in the 2θ range from 10 to 80 degrees. Based on the X-ray diffractogram of TiO_2 nanoparticles, several diffraction peaks are observed at the 2θ of 25.3, 37.7, 48.2, 54.1, 55.0, 62.3, 68.5, 70.3, and 75.3 degrees. In accordance with the JCPDS file No. 21-1272, the aforementioned peaks are respectively assigned to Miller indices of (101), (004), (200), (105), (211), (204), (116), (220), and (215), corresponding to anatase phase of TiO_2 [1-3]. No other peaks are observed except those related to

[DOI: 10.22068/ijmse.4261]

TiO_2 nanoparticles, indicating that our fabricated sample is free of impurities and has high purity. The average dimension of TiO_2 nanoparticles was calculated by means of Equation 1, which is known as Debye–Scherrer's formula [4]:

$$D = \frac{K\lambda}{\beta \cos\theta} \quad (1)$$

Where D stands for the mean size of the particles, K signifies the Scherrer constant with the value of 0.98, λ represents the X-ray wavelength equal to 1.541 Å, and β denotes the full width at half maximum (FWHM). By taking the sharpest peak at 25.3 degrees into account for the calculation of the mean size of TiO_2 nanoparticles, a value of 10.92 nm was obtained for this sample.

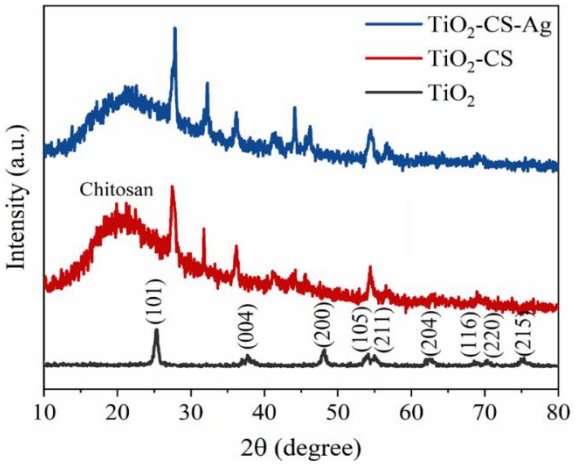

Fig. 1. XRD patterns of TiO_2, TiO_2-CS, and TiO_2-CS-Ag in the 2θ range from 10 to 80 degrees

Compositing TiO_2 nanoparticles with chitosan has resulted in some changes in their XRD pattern (Figure 1). Accordingly, a broad peak has appeared at approximately 20 degrees, attributed to amorphous chitosan [5, 6]. Moreover, some of the diffraction peaks relevant to TiO_2 nanoparticles are observed. Using Equation 1, an average particle size of 3.43 nm was obtained for TiO_2-CS, indicating that the compositing process can reduce nanoparticle size. The inclusion of Ag particles in the TiO_2-CS nanocomposite has had a negligible effect on its XRD pattern (Figure 1). Accordingly, the broad peak at 20°, relevant to amorphous chitosan, and the diffraction peaks of TiO_2 nanoparticles are visible. No peak pertinent to Ag particles can be seen, which may be as a result of high dispersion of Ag particles within the nanocomposite or overlapping the XRD peaks of Ag with TiO_2 [17, 18]. Among all the fabricated samples, the smallest size was achieved for TiO_2-CS-Ag nanocomposite (3.01 nm); therefore, this sample could benefit from a high surface-to-volume ratio. FTIR spectroscopy was another characterisation technique used to probe the functional groups in the prepared samples. According to Figure 2a exhibiting the FTIR spectrum of TiO_2 nanoparticles, a broad peak can be observed at the wavenumber of 3455 cm^{-1}, which arises from the hydroxyl (O-H) groups related to water molecules [7, 8]. The peak at 2920 cm^{-1} is pertinent to the stretching vibration of C-H [6]. The peak at 2360 cm^{-1} corresponds to physisorbed carbon dioxide (CO_2) molecules present in air onto the sample [13]. In addition to peaking at ~3455 cm^{-1}, the one centered at 1627 cm^{-1} is correlated to water molecules [12]. The characteristic peaks relevant to the Ti-O tensile and Ti-O-Ti bridging modes typically appear in the wavenumber varying from 400 to 1000 cm^{-1} [11]; hence, the absorption band at 500 cm^{-1} is ascribed to TiO_2.

For the TiO_2-CS nanocomposite (Figure 2b), the peaks at 1731 and 1064 cm^{-1} respectively relevant to the absorption bands of C=O and C-O, originate from chitosan [6]. Moreover, the absorption band corresponding to TiO_2 nanoparticles in the nanocomposite is observed at 500 cm^{-1}. Figure 2c illustrates the FTIR spectrum of TiO_2-CS-Ag nanocomposite. Accordingly, all the absorption bands interpreted for its counterpart without Ag (Figure 2b) can be seen. In addition to those peaks, a well-defined peak is observed at about 1388 cm^{-1}, which is attributed to Ag^+-N coordination bonds [9].

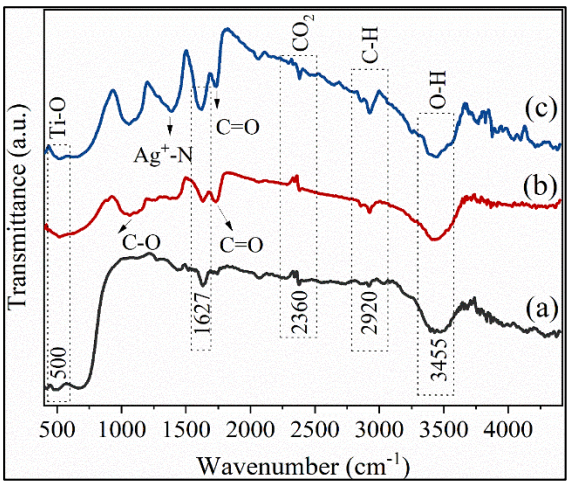

Fig. 2. FTIR spectra of a) TiO_2, b) TiO_2-CS, and c) TiO_2-CS-Ag

Figure 3 represents FESEM images of the prepared samples. According to Figure 3a, the FESEM image of TiO_2 shows spherical-shaped nanoparticles.

[DOI: 10.22068/ijmse.4261]

The size of the clusters composed of TiO_2 nanoparticles changes from 58 nm to 344.9 nm. Compositing TiO_2 nanoparticles with chitosan has caused a negligible effect on their morphology. The clusters of spherical-shaped TiO_2 nanoparticles are also found for the TiO_2-CS nanocomposite (Figure 3b), whose size varies from 40.65 nm to 120.9 nm. Comparing the morphology of TiO_2 and TiO_2-CS (see Figures 3a and 3b) demonstrates that the compositing process could cause more agglomeration among clusters. Without chitosan, the TiO_2 nanoparticles are more evenly distributed.
Introduction of Ag particles into the TiO_2-CS nanocomposite matrix has significantly altered its morphology. Flower-like species consisting of polygonal nanoparticles are observed in the FESEM image of the TiO_2-CS-Ag nanocomposite (Figure 3c). The size of the polygonal nanoparticles is 89.02-341.2 nm.
As shown in Figure 4a, the EDXS pattern of TiO_2 nanoparticles shows a pronounced peak for oxygen (O) at about 0.5 keV. In addition, the characteristic peaks of the titanium (Ti) element are easily found at approximately 0.5 and 4.5 keV. The peaks of oxygen and titanium elements originate from the TiO_2 nanoparticles. Like TiO_2, the EDXS pattern of TiO_2-CS nanocomposite reveals the peaks of oxygen and titanium elements relevant to TiO_2 nanoparticles (Figure 4b). Moreover, the carbon (C) peak can be detected at about 0.25 keV. The peaks of carbon and oxygen are associated with the presence of chitosan in the nanocomposite. For the TiO_2-CS-Ag nanocomposite (Figure 4c), the peaks of oxygen and titanium, indicative of TiO_2 nanoparticles, and the peaks of carbon and oxygen, related to chitosan, are clearly distinguished. Additionally, the conspicuous peaks of the silver (Ag) element are discernible at about 3.0 and 3.75 keV.

3.2. Specific Surface Area Investigation

The specific surface areas of TiO_2, TiO_2-CS, and TiO_2-CS-Ag were examined by BET analysis. Figure 5 demonstrates the nitrogen absorption-desorption isotherms for the prepared samples. Additionally, the BET results are listed in Table 1.

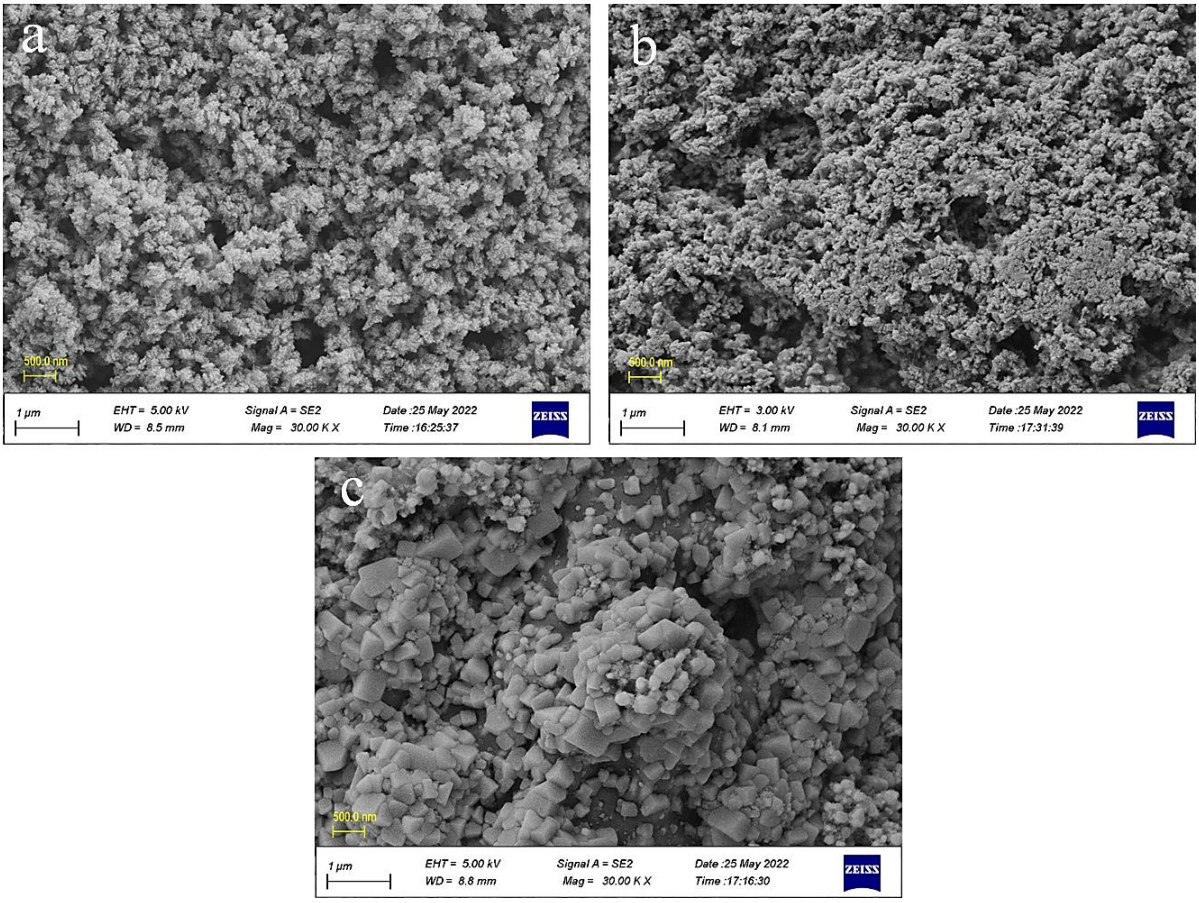

Fig. 3. The FESEM images of a) TiO_2, b) TiO_2-CS, and c) TiO_2-CS-Ag at various magnifications

[DOI: 10.22068/ijmse.4261]

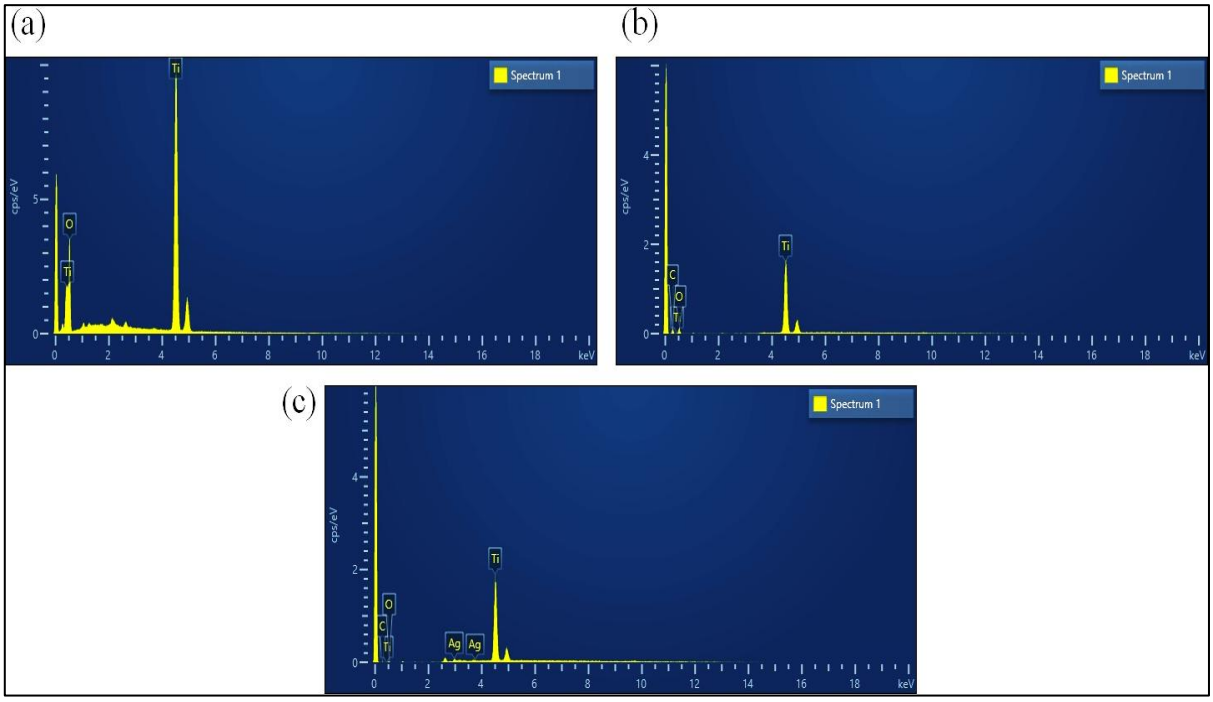

Fig. 4. The EDXS patterns of a) TiO_2, b) TiO_2-CS, and c) TiO_2-CS-Ag

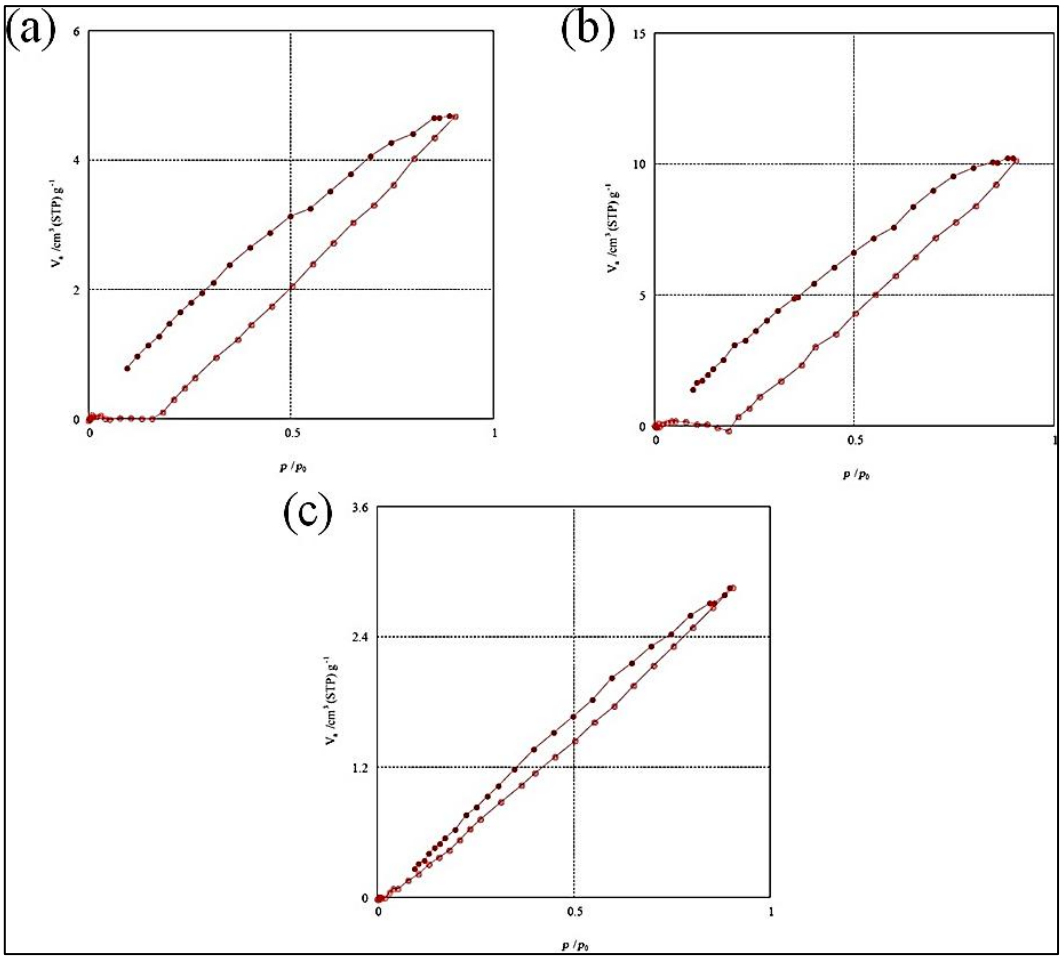

Fig. 5. Nitrogen absorption-desorption isotherm of a) TiO_2, b) TiO_2-CS, and c) TiO_2-CS-Ag

[DOI: 10.22068/ijmse.4261]

Table 1. Data obtained from the BET analysis conducted for TiO_2, TiO_2-CS, and TiO_2-CS-Ag

Sample	Mean pore diameter (nm)	Effective pore volume (cm^3/g)	Effective surface area (m^2/g)
TiO_2	2020.7	0.0072335	0.014319
TiO_2-CS	85304	0.015655	0.00073408
TiO_2-CS-Ag	106.48	0.0044144	0.16582

Accordingly, all the samples exhibit a mean pore diameter exceeding 50 nm, indicating they are macropores. The average pore diameter achieved for TiO_2 nanoparticles is 2020.7 nm. Compositing TiO_2 with chitosan has resulted in an increment in mean pore diameter. In this regard, the sample with chitosan shows an average pore diameter of 85304 nm, which is higher than that of the samples without chitosan (TiO_2 nanoparticles) and with chitosan and Ag (TiO_2-CS-Ag nanocomposite). Introduction of Ag resulted in a significant decrease in mean pore diameter, and the sample containing both chitosan and Ag showed the lowest mean pore diameter. In terms of effective surface area, the highest value is obtained for TiO_2 nanoparticles composited with chitosan and included with Ag. This can be tied to the nanocomposite dimension, where the least amount was observed for TiO_2-CS-Ag, as evidenced by XRD analysis. A smaller size provides more active surface area. Interestingly, the TiO_2-CS nanocomposite had a lower effective surface area than its counterpart without chitosan. In addition to BET, BJH analysis was performed to determine the pore-size distribution. According to BJH absorption (Figure 6a) and desorption (Figure 6b) curves of TiO_2 nanoparticles, both mesopores (2–50 nm) and macropores (>50 nm) can be found. Compositing TiO_2 with chitosan had a negligible effect on pore size distribution.

Like TiO_2, the BJH absorption (Figure 6c) and desorption (Figure 6d) curves of TiO_2-CS nanocomposite demonstrate a mixture of mesopores and macropores. Mixing TiO_2 nanoparticles with CS has increased pore volume. Introduction of Ag within TiO_2-CS nanocomposite decreased the pore volume. The TiO_2-CS-Ag nanocomposite also showed a combination of mesopores and macropores (Figures 6e, f).

3.3. Antibacterial Activity Measurements

Antibacterial activities of TiO_2, TiO_2-CS, and TiO_2-CS-Ag against E.coli and S.aureus, respectively, as gram-negative and gram-positive bacteria, were examined by means of the disk diffusion method. This technique is typically performed by spreading the microorganism on an agar culture medium and then placing the antibacterial agent as a spot on the medium. Antibacterial agents are expected to inhibit germination and prevent the growth of microorganisms. The circular area around the spot of the antibacterial agent, or, in other words, the zone of inhibition, is measured as a parameter for assessing the agent's effectiveness. A larger inhibition zone indicates greater susceptibility of the microorganism to the antibacterial agent.

Figure 7 demonstrates the disk diffusion test carried out for TiO_2, TiO_2-CS and TiO_2-CS-Ag against E.coli. Accordingly, the largest inhibition zone is observed after 24 hours for the TiO_2-CS-Ag nanocomposite among all the samples. As a result, TiO_2-CS-Ag exhibits high antibacterial activity against E. coli. No zone of inhibition can be detected for the blank sample, nor for TiO_2 nanoparticles. Therefore, they lack any antibacterial activity against E.coli. On the other hand, compositing TiO_2 nanoparticles with chitosan has resulted in a zone of inhibition smaller than that observed for the TiO_2-CS-Ag nanocomposite. High antibacterial activity of TiO_2-CS-Ag nanocomposite against E. coli can be related to two reasons, one of which is the presence of silver particles acting as powerful antibacterial agents against both gram-positive and gram-negative bacteria [10]. The other reason is the role of both chitosan and Ag in reducing the size of TiO_2 nanoparticles and subsequently, increasing their surface area, as evidenced by both XRD and BET analyses.

In addition to E.coli, the antibacterial activity of our prepared samples was investigated against S.aureus, a gram-positive bacterium. Figure 8 exhibits the zone of inhibition recorded for TiO_2, TiO_2-CS and TiO_2-CS-Ag against S. aureus after 24 hours.

Accordingly, the largest inhibition zone is observed with the TiO_2-CS-Ag nanocomposite, indicating that this sample could serve as an antibacterial agent against Gram-positive bacteria. Like the TiO_2-CS-Ag nanocomposite, its Ag-free counterpart also shows antibacterial activity against S.aureus. On the other hand, no inhibition zone is observed

[DOI: 10.22068/ijmse.4261]

for TiO_2 nanoparticles; consequently, this sample exhibits no antibacterial activity against S.aureus. The results of antibacterial activity measurements corroborate that the TiO_2-CS-Ag nanocomposite could be an ideal antibacterial agent against both gram-negative and gram-positive bacteria.

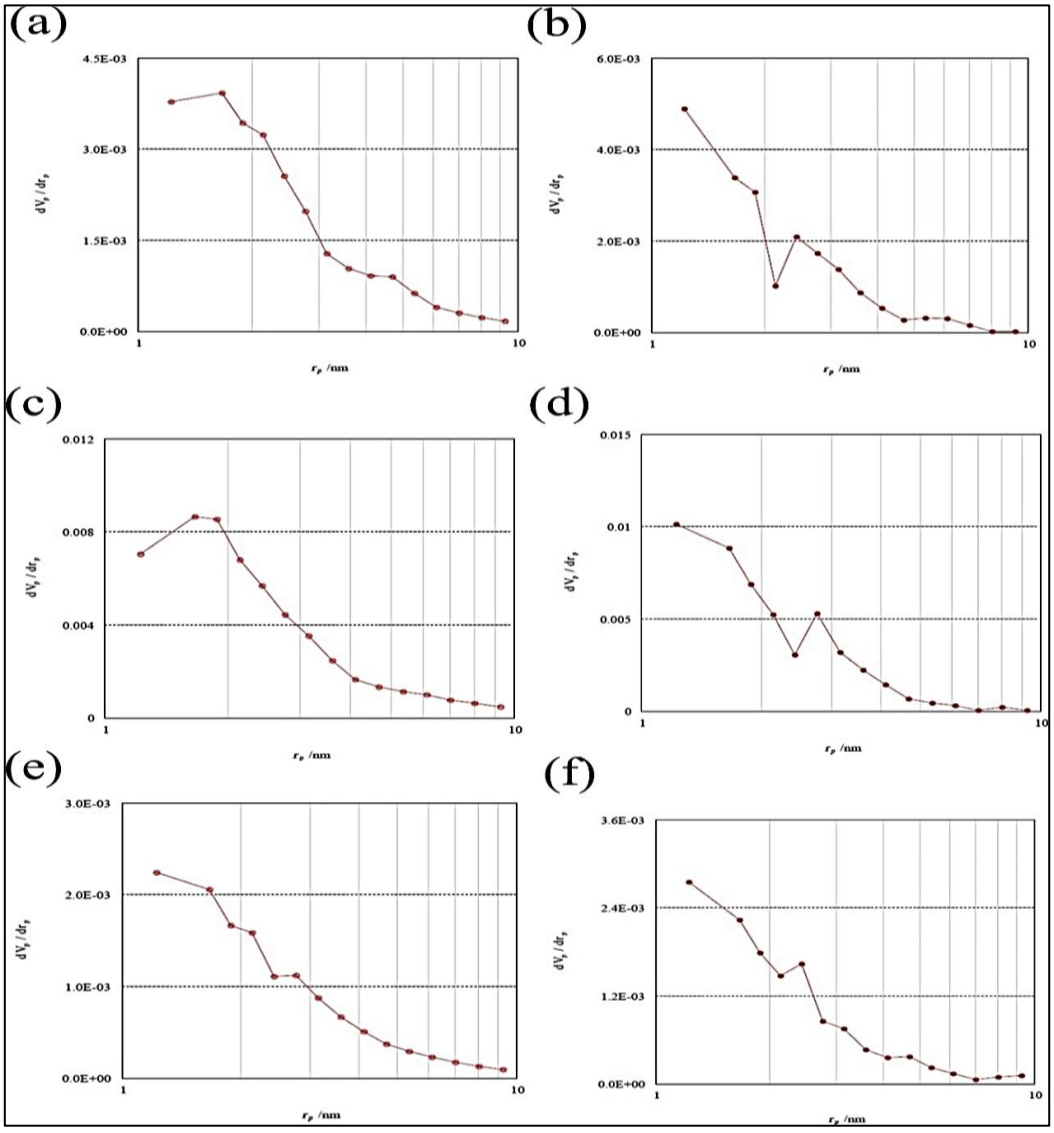

Fig. 6. The BJH curves for a,b) TiO_2, c,d) TiO_2-CS, and e,f) TiO_2-CS-Ag. For each sample, the first and second curves are the absorption and desorption curves, respectively

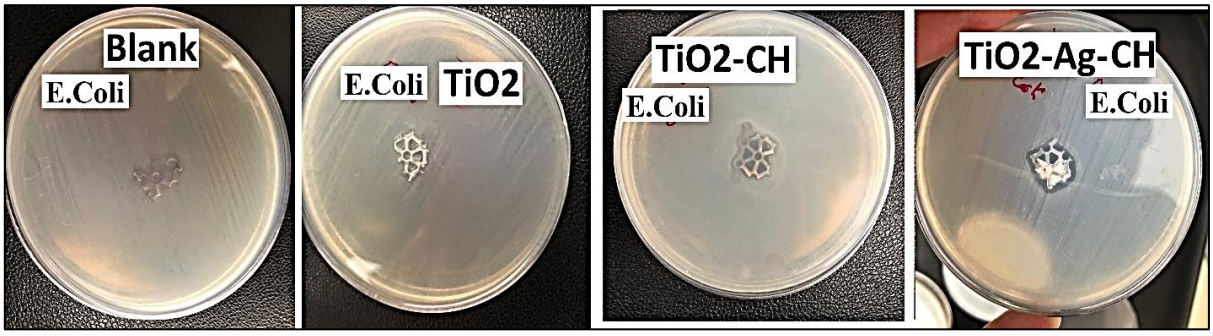

Fig. 7. Zone of inhibition obtained for the disks without case study samples and with TiO_2, TiO_2-CS and TiO_2-CS-Ag against E.coli

[DOI: 10.22068/ijmse.4261]

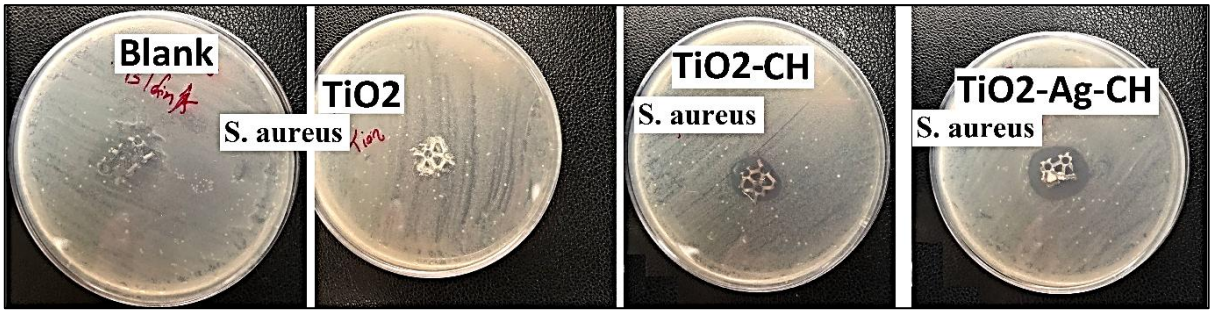

Fig. 8. Zone of inhibition recorded for the disks without case study samples and with TiO_2, TiO_2-CS and TiO_2-CS-Ag against S.aureus

4. CONCLUSIONS

In this work, TiO_2 nanoparticles and their nanocomposites, including TiO_2-CS and TiO_2-CS-Ag, were synthesised to evaluate their antibacterial activity. All the characterization tests were used to verify the synthesis of the samples. In accordance with XRD test, including solely chitosan or both chitosan and Ag into TiO_2 nanoparticles changed their X-ray diffractogram. In addition, the nanocomposites exhibited a smaller average size than the nanoparticles. FTIR spectroscopy confirmed the preparation of the samples, with characteristic peaks for TiO_2, chitosan, and Ag observed. TiO_2 nanoparticles and their composite with chitosan showed almost identical morphologies. However, the inclusion of Ag into the TiO_2-CS nanocomposite completely changed its morphology. Among all the samples, only TiO_2-CS and TiO_2-CS-Ag nanocomposites showed antibacterial activity against E.coli and S.aureus, with the highest effectiveness observed for the Ag-containing nanocomposite. The excellent antibacterial activity of TiO_2-CS-Ag nanocomposites was attributed to the presence of Ag particles and their high surface area, as confirmed by BET analysis.

The results of our study put forward that TiO_2-CS-Ag nanocomposites could be ideal for medical applications. They can be adapted to address health issues caused by E.coli and S.aureus.

REFERENCES

[1] Nagaraj, G., et al., Facile synthesis of improved anatase TiO_2 nanoparticles for enhanced solar-light driven photocatalyst. SN Applied Sciences, 2020. 2: p. 1-9.

[2] Jamil, S. and M. Fasehullah, Effect of temperature on structure, morphology, and optical properties of TiO_2 nanoparticles. Mater Innov, 2021. 1(01): p. 22-8.

[3] Mallick, S., et al., PLA-TiO_2 nanocomposites: Thermal, morphological, structural, and humidity sensing properties. Ceramics International, 2018. 44(14): p. 16507-16513.

[4] Tamarani, A., R. Zainul, and I. Dewata. Preparation and characterization of XRD nano Cu-TiO_2 using sol-gel method. in Journal of Physics: Conference Series. 2019. IOP Publishing.

[5] Castillo, B.E., et al., Potential use of chitosan-TiO_2 nanocomposites for the electroanalytical detection of imidacloprid. Polymers, 2022. 14(9): p. 1686.

[6] Taspika, M., et al., Influence of TiO_2/Ag particles on the properties of chitosan film. Advances in Natural Sciences: Nanoscience and Nanotechnology, 2020. 11(1): p. 015017.

[7] El-Desoky, M., et al., Synthesis, structural and electrical properties of PVA/TiO_2 nanocomposite films with different TiO_2 phases prepared by sol–gel technique. Journal of Materials Science: Materials in Electronics, 2020. 31(20): p. 17574-17584.

[8] Deyab, M., A.A. Nada, and A. Hamdy, Comparative study on the corrosion and mechanical properties of nano-composite coatings incorporated with TiO_2 nanoparticles, TiO_2 nano-tubes, and ZnO nanoflowers. Progress in Organic Coatings, 2017. 105: p. 245-251.

[9] Zhang, B., Y. Luo, and Q. Wang, Development of silver/α-lactalbumin nanocomposites: a new approach to reduce silver toxicity. International Journal of Antimicrobial Agents, 2011. 38(6): p. 502-509.

[10] Li, J., Xie, B., Xia, K., Li, Y., Han, J. and Zhao, C., Enhanced antibacterial activity of silver doped titanium dioxide-chitosan composites under visible light. Materials, 2018. 11(8): p.1403.

[DOI: 10.22068/ijmse.4261]

[11] Dong, Z., Li, R. and Gong, Y., Antibacterial and freshness-preserving mechanisms of chitosan-nano-TiO_2-nano-Ag composite materials. Coatings, 2021. 11(8): p.914.
[12] Zafar, N., Uzair, B., Niazi, M.B.K., Samin, G., Bano, A., Jamil, N., Sajjad, S. and Menaa, F., Synthesis and characterization of potent and safe ciprofloxacin-loaded Ag/TiO_2/CS nanohybrid against mastitis causing E.coli. Crystals, 2021, 11: p. 319.
[13] Abutalib, M.M. and Rajeh, A.J.P.T., Enhanced structural, electrical, mechanical properties and antibacterial activity of Cs/PEO doped mixed nanoparticles (Ag/TiO_2) for food packaging applications. Polymer Testing, 2021. 93: p. 107013.
[14] Usman Khan, M., Rehman, W., Bibi, S., Alanazi, M.M., Alanazi, A.S., Rasheed, L., Khan, S., Tariq Gillani, S.U. and Tauqeer, A., Synthesis, characterization, and antimicrobial and nematicidal activities of chitosan-based silver-doped titanium dioxide. ACS omega, 2023. 8: pp. 19341-19350.
[15] Hoang, T.D., Nguyen, T.C., Doan, T.T., Ngo, T.D., Nguyen, T.Y., Ngo, B.T., Tran, T.T. and Le, T.L., Preparation and photocatalytic and antibacterial properties of polyvinyl alcohol/chitosan/TiO_2@Ag electrospun nanofibers. Thin Solid Films, 2024. 797: p. 140344.
[16] Lin, D., Yang, Y., Wang, J., Yan, W., Wu, Z., Chen, H., Zhang, Q., Wu, D., Qin, W. and Tu, Z., Preparation and characterization of TiO_2-Ag loaded fish gelatin-chitosan antibacterial composite film for food packaging. International Journal of Biological Macromolecules, 2020. 154: pp. 123-133.
[17] Rana, A., Parashar, S., Singh, D., Singh, K., Chanda, D., Pal, A., Srivastava, R. and Sharma, S.N., Exploring the dermal safety of green-synthesized Ag–TiO_2 nanocomposites for topical applications. RSC advances, 2025, 15(12): pp. 9320-9334.
[18] Zhang, C., Hua, H., Liu, J., Han, X., Liu, Q., Wei, Z., Shao, C. and Hu, C., Enhanced photocatalytic activity of nanoparticle-aggregated Ag–AgX (X= Cl,Br)@TiO_2 microspheres under visible light. Nano-Micro Letters, 2017, 9(4): p. 49.

[DOI: 10.22068/ijmse.4261]